Nanoscale

PAPER

View Article Online
View Journal | View Issue

Cite this: *Nanoscale*, 2025, **17**, 26123

Reductant-selected formation of copper nanoclusters with crystallization-induced emission enhancement performance

Ye Tian,† Wenlong Xu,† Jian Zhu,† Jiayu Lu, Zhaohang Chen, Fakhari Alam, Honglei Shen,* Xi Kang * and Manzhou Zhu

Received 16th August 2025,
Accepted 16th October 2025

DOI: 10.1039/d5nr03478g

rsc.li/nanoscale

The rational design of emissive copper nanoclusters presents a significant challenge due to their inherent instability and complex coordination chemistry. In this study, we propose a reductant-mediated strategy to precisely regulate the atomic structure and photophysical properties of copper nanoclusters. The strong reductant sodium borohydride ($NaBH_4$) yields a non-emissive $Cu_{14}(DMP)_6(PPh_2py)_8$ species, while the mild reductant borane *tert*-butylamine complex leads to the formation of a tetrahedral $Cu_4(PPh_2py)_4Cl_2$ cluster, which exhibits a remarkable crystallization-induced emission enhancement (CIEE). Hirshfeld surface analysis of the Cu_4 nanocluster indicates that multiple non-covalent interactions —such as H···H, C–H···π, and Cl···H contacts—stabilize the molecular packing, effectively suppressing non-radiative decay pathways and contributing to the CIEE phenomenon. This work highlights the crucial role of reductants in modulating copper nanocluster structures and offers novel insights into the design of efficient copper-based emitters.

Introduction

Ligand-protected copper (Cu) nanoclusters represent a critical subclass of metal nanoclusters with immense potential for applications in catalysis, sensing, and photonics.[1–8] Their unique quantum size effects, discrete electronic states, and structure-dependent physicochemical properties contribute to this promise. Recent advances in synthetic chemistry have enabled the preparation of atomically precise Cu nanoclusters with well-defined core–shell architectures, establishing a foundation for rationally designing functional Cu-based nanomaterials.[9–13] However, controllable synthesis and property modulation of Cu nanoclusters remain significant challenges. Unlike gold and silver counterparts, copper clusters exhibit a wide variety of coordination modes and are generally less stable and more prone to oxidation.[12,14–22] These factors hinder precise control over atomic composition and surface coordination structures,[23,24] making the synthesis of stable Cu nanoclusters with superior physicochemical properties essential for both fundamental studies and practical applications.

Photoluminescence (PL) is among the most intriguing features of Cu nanoclusters, characterized by their strong emissions, significant Stokes shifts, and long excited-state lifetimes.[12,25–32] These properties make them promising candidates for optoelectronic and luminescent devices. To enhance the PL performance of Cu nanoclusters, strategies such as ligand modification,[33–35] heteroatom doping,[36–38] aggregation-induced emission (AIE),[39–44] and environmental tuning (*e.g.*, solvent,[15,45,46] pH,[47] and temperature[48]) have been explored. Crystallization-induced emission enhancement (CIEE), a specialized form of AIE, has proven particularly effective for improving Cu nanocluster emission.[27,49–52] In the crystalline state, ordered molecular packing strengthens intermolecular interactions while restricting intramolecular vibrations/rotations, thereby suppressing non-radiative decay and enhancing radiative recombination.[49–52] Despite this progress, a fundamental question remains unresolved: how can copper cluster formation be precisely directed during nucleation and growth to yield atomically defined structures with tailored luminescence properties? In this regard, the choice of reducing agents—a critical yet underexplored synthetic parameter —may serve as a powerful tool for guiding the structural evolution and emission characteristics of Cu nanoclusters.

Herein, we demonstrate that the reducing agent (sodium borohydride, $NaBH_4$, *vs.* borane *tert*-butylamine complex, TBAB) profoundly influences the formation and PL behavior of Cu nanoclusters. Specifically, $NaBH_4$ yields non-emissive

Department of Chemistry and Centre for Atomic Engineering of Advanced Materials, Key Laboratory of Structure and Functional Regulation of Hybrid Materials of Ministry of Education, Anhui Province Key Laboratory of Chemistry for Inorganic/Organic Hybrid Functionalized Materials, Anhui University, Hefei, Anhui 230601, P. R. China. E-mail: shenhonglei_chem@163.com, kangxi_chem@ahu.edu.cn
† These authors contributed equally to this work.

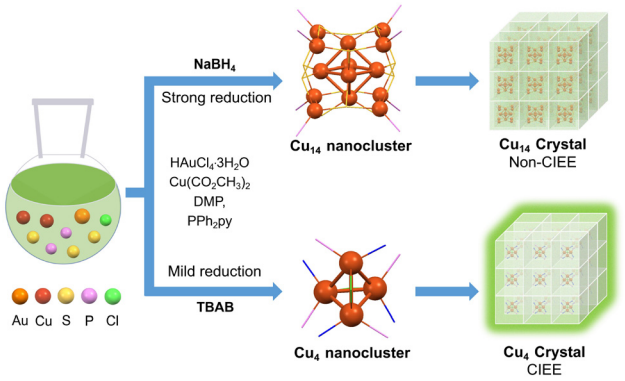

Scheme 1 Illustration of the reductant-selected formation of copper nanoclusters and their different PL behavior in the crystal state.

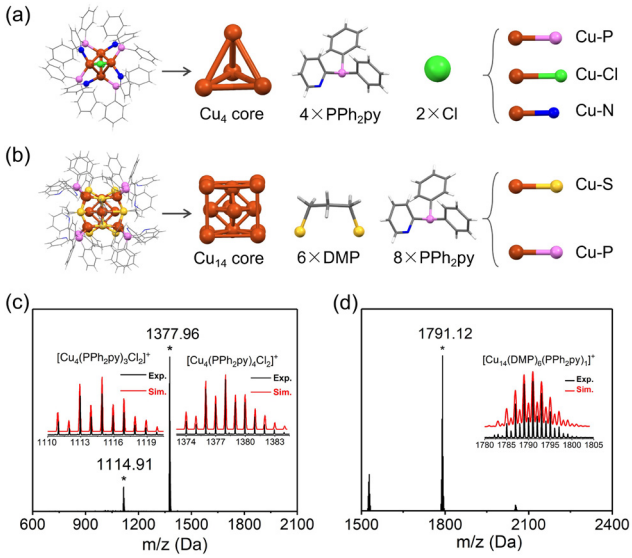

Fig. 1 Structural anatomy of (a) Cu_4 and (b) Cu_{14} nanoclusters. Positive-mode ESI-MS spectrum of (c) Cu_4 and (d) Cu_{14} nanoclusters. Insets: isotope patterns of experimental (black) and simulated (red) spectra of corresponding nanoclusters. Color legend: brown = Cu; yellow = S; pink = P; green = Cl; blue = N. For clarity, C and H atoms are shown in wireframe mode.

$Cu_{14}(DMP)_6(PPh_2py)_8$ (Cu_{14}), while TBAB generates tetrahedral $Cu_4(PPh_2py)_4Cl_2$ (Cu_4), which exhibits bright emission in both solution and solid states with pronounced CIEE (Scheme 1). Notably, embedding Cu_4 into a poly(methyl methacrylate) (PMMA) matrix *via* sol–gel processing enhances PL intensity and increases the PL quantum yield (PLQY) nearly 20-fold compared to the solution state. This improvement arises from the reduced non-radiative decay, mediated by intermolecular non-covalent interactions (H···H, C–H···π, and Cl···H interactions). This work highlights the pivotal role of reducing agents in directing Cu nanocluster structures, offering new insights for designing high-performance luminescent copper nanomaterials.

Results and discussion

The synthetic protocols for Cu_{14} and Cu_4 nanoclusters are highly similar, both employing a one-pot reduction strategy using Au–Cu–DMP–PPh_2py complexes as precursors. The critical distinction arises from the choice of reducing agent: Cu_{14} is synthesized with $NaBH_4$, while Cu_4 is produced using TBAB (see the SI for detailed procedures). This variation in reductant strength directly influences cluster formation. $NaBH_4$, a stronger reductant, accelerates metal aggregation, leading to the formation of a larger Cu_{14} cluster. Conversely, TBAB results in a gentler reduction, forming a smaller tetrahedral Cu_4 cluster. Notably, the synthesis of Cu_{14} is consistent with our previous work, and the structure of Cu_4 clusters is similar to those reported in earlier studies, despite different synthetic methods.[39,53] Both nanoclusters were crystallized *via* a CH_2Cl_2/*n*-hexane diffusion method, yielding high-quality crystals within one week that were suitable for single-crystal X-ray diffraction (SC-XRD) analysis.

The atomic structures of the Cu_4 and Cu_{14} nanoclusters were determined by SC-XRD. The Cu_4 nanocluster crystallizes in a monoclinic crystal system (space group: $P2_1/c$), with two pairs of enantiomers present in each unit cell (Fig. S1 and Table S1). As illustrated in Fig. 1a, the nanocluster features a tetrahedral Cu_4 core that is stabilized by four phosphine (PPh_2py) ligands and two chloride (Cl) ligands. Each Cu atom in the core exhibits a mixed coordination environment involving N (from the ring of PPh_2py), P, and Cl ligands, collectively rigidifying the core–shell framework (Fig. 1a). In contrast, the Cu_{14} nanocluster crystallizes in a triclinic crystal system (space group: $P\bar{1}$), with one cluster per unit cell (Fig. S2, Table S2). The cubic Cu_{14} core is protected by six DMP ligands and eight PPh_2py ligands (Fig. 1b), with a simpler coordination sphere dominated by S (from DMP) and P sites. The absence of nitrogen or halogen coordination in Cu_{14} likely reduces structural rigidity compared to Cu_4. Besides, Cu_4 exhibits longer Cu–Cu bond lengths and shorter Cu–P bond lengths compared to Cu_{14} (Table S3), which directly influence its photophysical properties. The shorter Cu–P bonds enhance orbital overlap between copper atoms and phosphine ligands, facilitating ligand-to-metal charge transfer (LMCT). The longer Cu–Cu bonds weaken vibrational coupling between copper atoms, reducing non-radiative transitions. Additionally, the Cu–N and Cu–Cl interactions in Cu_4 enhance molecular rigidity and intermolecular interactions, contributing to its stability and superior optical performance.

Electrospray ionization mass spectrometry (ESI-MS) confirmed the molecular compositions. For Cu_4, the dominant peak at m/z = 1377.9 corresponds to $[Cu_4(PPh_2py)_4Cl_2]^+$, while the minor peak at m/z = 1114.9 matches $[Cu_4(PPh_2py)_3Cl_2]^+$ (Fig. 1c). Experimental isotope patterns align precisely with simulated patterns, validating the crystal structure. Similarly, ESI-MS analysis of Cu_{14} verified its composition and purity (Fig. 1d).

X-ray photoelectron spectroscopy (XPS) analysis confirmed the presence of expected elements in Cu_4 and Cu_{14} nanoclusters (Fig. S3 and S4). High-resolution Cu 2p spectra reveal

mixed Cu^{+}/Cu^{0} species in Cu_{14}, with peaks at 932.5 eV and 952.4 eV. In contrast, Cu_4 exhibits higher binding energies in Cu 2p spectra (Fig. S5), indicative of elevated Cu oxidation states. Cu LMM Auger electron spectroscopy further confirms that Cu_4 contains more oxidized Cu species than Cu_{14} (Fig. S6). These differences correlate with reductant strength: the milder reducing environment of TBAB promotes partial oxidation in Cu_4, while $NaBH_4$ drives Cu_{14} toward reduced states. By combining the ESI-MS and XPS results, the Cu_4 nanocluster should be in a "+2"-charge state while Cu_{14} is an electrically neutral molecule. However, both clusters presented "+1"-charged signals in the mass spectra, suggesting a potential electron-gaining or electron-losing behavior of the two clusters in the mass spectrometry environment.

Optical properties were investigated *via* UV-vis and PL spectroscopy. The UV-vis spectrum of Cu_4 shows a shoulder peak at 265 nm and two prominent bands at 315 and 390 nm. In contrast, Cu_{14} displays a dominant absorption peak at 265 nm, accompanied by a weaker shoulder at 350 nm (Fig. 2a). The main absorption peak of Cu_4 at 390 nm represents a significant 40 nm redshift compared to Cu_{14}, reflecting structural differences in core–shell geometry and electronic configurations of the two nanoclusters.

PL measurements reveal stark contrasts of the two nanoclusters in the solution state: Cu_{14} is non-emissive in solution, while Cu_4 exhibits strong emission with the emissive peak centered at 573 nm (Fig. 2b). In the crystalline state, Cu_{14} remains virtually non-emissive, while Cu_4 shows a significant increase in PL intensity (Fig. S7). In this context, the crystalline state of Cu_4 nanocluster demonstrates markedly enhanced PL emission, with emission intensity greatly surpassing that observed in solution, demonstrating its CIEE behavior.

To evaluate the PL behavior of Cu_4 in monodisperse (solution), amorphous (film), and crystalline states, we fabricated a Cu_4-based composite film using PMMA as the polymer matrix. Under 365 nm UV excitation, all samples emitted visible emission with distinct color shifts dependent on their physical state (Fig. 3a). The corresponding CIE chromaticity coordinates confirmed a progressive color shift from yellow to green, with coordinates of (0.46, 0.51) for the solution, (0.42, 0.52) for the film, and (0.37, 0.53) for crystalline Cu_4 (Fig. 3b). Besides, steady-state fluorescence tests of Cu_4 crystals demonstrated

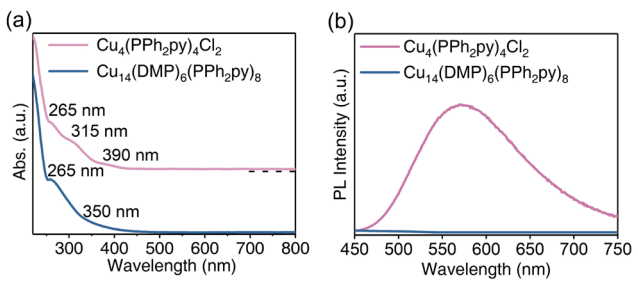

Fig. 2 (a) UV-vis spectra and (b) PL spectra of Cu_4 (red) and Cu_{14} (blue) nanoclusters in CH_2Cl_2 solution (λ_{ex} = 365 nm). All samples were measured at the same optical density of 0.05.

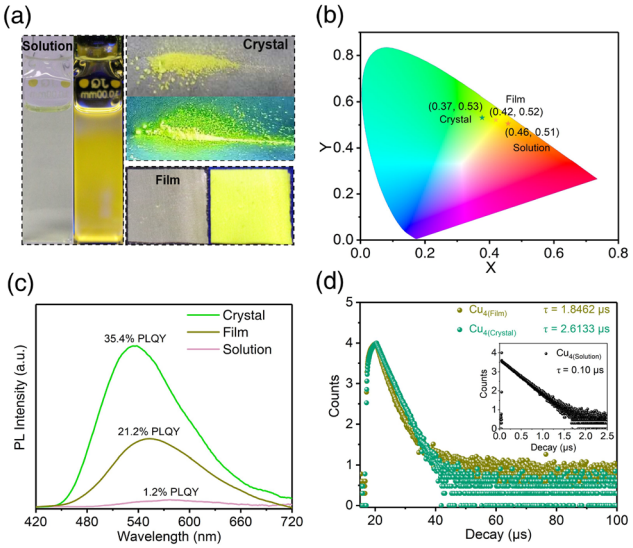

Fig. 3 (a) Photographs of Cu_4 samples under UV illumination (365 nm) in solution, film, and crystal states. (b) CIE chromaticity coordinates of Cu_4 samples. (c) PL intensity and (d) fluorescence lifetime decay profiles of Cu_4 samples.

that such a nanocluster was singly emissive (Fig. S8). Quantitative photophysical measurements revealed that the solution-state Cu_4 exhibited weak emission, with a PLQY of only 1.2%. However, when embedded in the PMMA matrix, the PLQY increased substantially to 21.2%. This enhancement is attributed to the restriction of intramolecular motion through AIE, even in the amorphous state (Fig. 3c). Notably, the crystalline form exhibited the highest PLQY of 35.4%, indicative of a strong CIEE effect. Additionally, a PL emission intensity test was conducted to compare the stability of the Cu_4 cluster in both crystal and film states. The results demonstrate that both forms retain their PL properties after exposure to the atmosphere for three months (Fig. S9).

To elucidate the emission mechanism behind the Cu_4 nanocluster, we calculated the radiative (k_r) and non-radiative (k_{nr}) rate constants based on the measured PLQY and lifetime data (Table S4). Time-resolved fluorescence measurements revealed progressively increased lifetimes: 0.1 μs (solution), 1.8462 μs (film), and 2.6133 μs (crystal) (Fig. 3d). Notably, the k_{nr} values for both the Cu_4-based film and crystalline samples decreased by approximately one order of magnitude compared to the solution state. This dramatic reduction confirms that Cu_4 aggregation effectively suppresses non-radiative decay pathways, significantly enhancing the PL efficiency of the cluster materials.

In the Cu_4 crystal lattice, most PPh_2py phenyl rings engage in intercluster interactions: H···H (2.173–2.736 Å), C–H···π (2.883–3.146 Å), and Cl···H (2.705 Å) interactions (Fig. S10). To probe the molecular origins of the CIEE in Cu_4, we conducted Hirshfeld surface analysis and 2D fingerprint mapping to investigate the intermolecular interactions that influence the crystal packing. The d_{norm} surface reveals close short-range

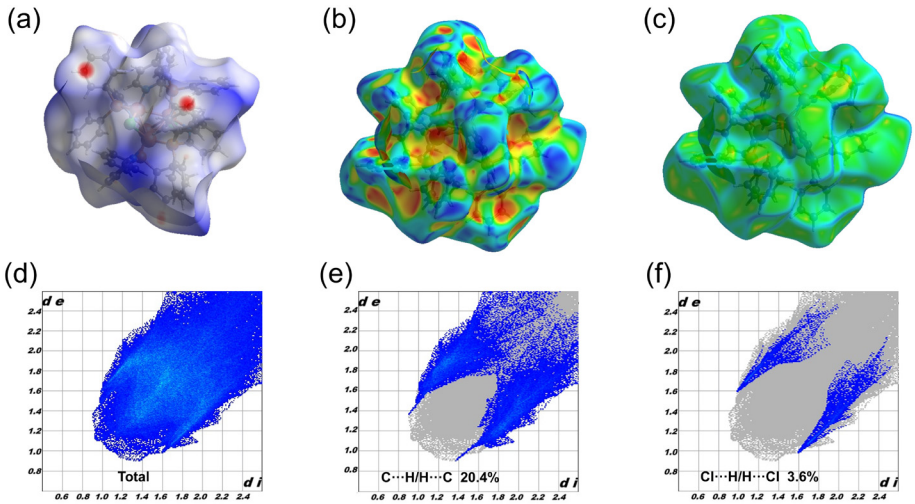

Fig. 4 Hirshfeld surface plots and 2D fingerprint plots of the Cu_4 cluster. Short contacts are shown in red. Long contacts are shown in blue. The white area represents the contacts with lengths equivalent to the sum of the van der Waals radii of interacting atoms. Hirshfeld surface analysis of Cu_4 in (a) d_{norm}, (b) shape index, and (c) curvedness. 2D fingerprinting plots of Cu_4 showing the (d) total interaction and proportion of (e) C···H/H···C and (f) Cl···H/H···Cl in the fingerprint.

contacts, particularly C–H···π (red dots) and Cl···H interactions (red circle) (Fig. 4a and Fig. S11). The shape index map displays complementary red/blue triangular features, indicative of C–H···π stacking interactions (Fig. 4b), while the curvedness map shows extended flat regions that further support the presence of these C–H···π contacts (Fig. 4c). Fingerprint analysis quantifies all intermolecular interactions (Fig. 4d), with C···H/H···C interactions dominating, emphasizing the crucial role of C–H···π interactions in stabilizing the crystal lattice (Fig. 4e). Additionally, Cl···H/H···Cl contacts suggest that chlorine–hydrogen interactions also serve as an auxiliary stabilizing factor (Fig. 4f). This dense network of non-covalent interactions rigidifies the structure, restricting intramolecular ligand rotation/vibration. By elevating the energy barrier for vibrational relaxation, these constraints suppress non-radiative decay pathways, thereby enhancing PL quantum efficiency and driving the pronounced CIEE behavior in Cu_4. Furthermore, Hirshfeld surface analysis of Cu_{14} reveals that its surface is mostly governed by weak intermolecular interactions, such as H···H and C–H···π interactions (Fig. S12). Compared to the Cu_4 cluster, interactions like Cl···H bonds were not present in the Cu_{14} surface, suggesting its significantly weaker intermolecular interactions and non-CIEE behavior.

Conclusion

In summary, we have developed a reductant-mediated strategy to control the structures and photophysical properties of copper nanoclusters. By varying the reducing agent from $NaBH_4$ to TBAB, we successfully obtained two structurally and optically distinct Cu nanoclusters: non-emissive Cu_{14} and highly luminescent Cu_4. Notably, Cu_4 exhibits a pronounced CIEE phenomenon, which is attributed to its rigid molecular environment in the crystalline state. This rigidity suppresses non-radiative decay through synergistic C–H···π and Cl···H interactions. Hirshfeld surface analysis and 2D fingerprint plots reveal that these non-covalent interactions form a compact and ordered network, providing structural insights into the mechanism behind the enhanced PL intensity. In addition to understanding structure–property correlations, the impressive luminescence and stability of Cu_4 in both crystalline and film forms emphasize its potential applications in light-emitting devices, chemical sensors, and other optoelectronic systems. This work highlights the critical role of reductants in tailoring the structure–property correlations of Cu nanoclusters and presents a feasible approach for the rational design of high-performance luminescent copper nanomaterials.

Author contributions

Y. Tian, W. Xu and J. Zhu conceived and carried out experiments. J. Lu, Z. Chen and F. Alam assisted in the synthesis and optical spectral measurements. H. Shen and X. Kang analyzed the data and wrote the paper. M. Zhu supervised the project.

Conflicts of interest

The authors declare no conflicts of interest.

Data availability

The data that support the findings of this study are available in the supplementary information (SI). Supplementary information is available. See DOI: https://doi.org/10.1039/d5nr03478g.

CCDC 2468154 contains the supplementary crystallographic data for this paper.[54]

Acknowledgements

We acknowledge the financial support from the NSFC (22371003, 22101001, and 22471001), the China Postdoctoral Science Foundation Funded Project (2024M760007), and the Scientific Research Program of Universities in Anhui Province (2022AH030009).

References

1 R. Jin, C. Zeng, M. Zhou and Y. Chen, *Chem. Rev.*, 2016, **116**, 10346–10413.
2 R. Jin, G. Li, S. Sharma, Y. Li and X. Du, *Chem. Rev.*, 2021, **121**, 567–648.
3 I. Chakraborty and T. Pradeep, *Chem. Rev.*, 2017, **117**, 8208–8271.
4 S. Li, J. Wei, Q. Yao, X. Song, J. Xie and H. Yang, *Chem. Soc. Rev.*, 2023, **52**, 1672–1696.
5 Q. Yao, M. Zhu, Z. Yang, X. Song, X. Yuan, Z. Zhang, W. Hu and J. Xie, *Nat. Rev. Mater.*, 2025, **10**, 89–108.
6 J. V. Rival, S. Chand, A. Jana, Nonappa, V. Biju, T. Pradeep, P. Rajamalli and E. S. Shibu, *Adv. Mater.*, 2025, **37**, 2507893.
7 B. Alamer, A. Sagadevan, M. Bodiuzzaman, K. Murugesan, S. Alsharif, R.-W. Huang, A. Ghosh, M. H. Naveen, C. Dong, S. Nematulloev, J. Yin, A. Shkurenko, M. Abulikemu, X. Dong, Y. Han, M. Eddaoudi, M. Rueping and O. M. Bakr, *J. Am. Chem. Soc.*, 2024, **146**, 16295–16305.
8 J. Lu, B. Shao, R.-W. Huang, L. Gutiérrez-Arzaluz, S. Chen, Z. Han, J. Yin, H. Zhu, S. Dayneko, M. N. Hedhili, X. Song, P. Yuan, C. Dong, R. Zhou, M. I. Saidaminov, S.-Q. Zang, O. F. Mohammed and O. M. Bakr, *J. Am. Chem. Soc.*, 2024, **146**, 4144–4152.
9 H. Zhao, C. Zhang, B. Han, Z. Wang, Y. Liu, Q. Xue, C.-H. Tung and D. Sun, *Nat. Synth.*, 2024, **3**, 517–526.
10 H. Zhao, C. Zhang, B.-L. Han, P. Mahato, C.-Z. Yang, P.-X. Yu, Z. Wang, C.-H. Tung and D. Sun, *Nano Lett.*, 2025, **25**, 9132–9138.
11 M. Chen, C. Guo, L. Qin, L. Wang, L. Qiao, K. Chi and Z. Tang, *Nano-Micro Lett.*, 2024, **17**, 83.
12 N. Zhang, Y. Li, S. Han, Y. Wei, H. Hu, R. Huo, C. Duan, J. Zhang, C. Han, G. Xie and H. Xu, *Angew. Chem., Int. Ed.*, 2023, **62**, e202305018.
13 A. Ghosh, R.-W. Huang, B. Alamer, E. Abou-Hamad, M. N. Hedhili, O. F. Mohammed and O. M. Bakr, *ACS Mater. Lett.*, 2019, **1**, 297–302.
14 S. Lee, M. S. Bootharaju, G. Deng, S. Malola, W. Baek, H. Häkkinen, N. Zheng and T. Hyeon, *J. Am. Chem. Soc.*, 2020, **142**, 13974–13981.
15 P.-P. Sun, B.-L. Han, H.-G. Li, C.-K. Zhang, X. Xin, J.-M. Dou, Z.-Y. Gao and D. Sun, *Angew. Chem., Int. Ed.*, 2022, **61**, e202200180.
16 J. D. Schneider, B. A. Smith, G. A. Williams, D. R. Powell, F. Perez, G. T. Rowe and L. Yang, *Inorg. Chem.*, 2020, **59**, 5433–5446.
17 T.-A. D. Nguyen, Z. R. Jones, D. F. Leto, G. Wu, S. L. Scott and T. W. Hayton, *Chem. Mater.*, 2016, **28**, 8385–8390.
18 M. K. Osei, S. Mirzaei, X. Bogetti, E. Castro, M. A. Rahman, S. Saxena and R. H. Sánchez, *Angew. Chem., Int. Ed.*, 2022, **61**, e202209529.
19 L. L.-M. Zhang and W.-Y. Wong, *Aggregate*, 2023, **4**, e266.
20 A. Baghdasaryan, C. Besnard, L. M. L. Daku, T. Delgado and T. Burgi, *Inorg. Chem.*, 2020, **59**, 2200–2208.
21 W. Drescher, C. Borner and C. Kleeberg, *New J. Chem.*, 2021, **45**, 14957–14964.
22 N. Frank, A. Dallmann, B. Braun-Cula, C. Herwig and C. Limberg, *Angew. Chem., Int. Ed.*, 2020, **59**, 6735–6739.
23 R. C. Maji, P. P. Das, A. Bhandari, S. Mishra, M. Maji, K. B. Ghiassi, M. M. Olmstead and A. K. Patra, *Chem. Commun.*, 2017, **53**, 3334–3337.
24 M.-L. Fu, I. Issac, D. Fenske and O. Fuhr, *Angew. Chem., Int. Ed.*, 2010, **49**, 6899–6903.
25 X. Kang and M. Zhu, *Chem. Soc. Rev.*, 2019, **48**, 2422–2457.
26 M. Olaru, E. Rychagova, S. Ketkov, Y. Shynkarenko, S. Yakunin, M. V. Kovalenko, A. Yablonskiy, B. Andreev, F. Kleemiss, J. Beckmann and M. Vogt, *J. Am. Chem. Soc.*, 2020, **142**, 373–381.
27 T. Li, Z. Qi, N. Zhang, X. Zhao, H. Li and X.-M. Zhang, *Adv. Funct. Mater.*, 2024, **34**, 2410361.
28 C.-L. Chan, K.-L. Cheung, W. H. Lam, E. C.-C. Cheng, N. Zhu, S. W.-K. Choi and V. W.-W. Yam, *Chem. – Asian J.*, 2006, **1**, 273–286.
29 H. Li, H. Zhai, C. Zhou, Y. Song, F. Ke, W. W. Xu and M. Zhu, *J. Phys. Chem. Lett.*, 2020, **11**, 4891–4896.
30 N. Zhang, H. Hu, L. Qu, R. Huo, J. Zhang, C. Duan, Y. Meng, C. Han and H. Xu, *J. Am. Chem. Soc.*, 2022, **144**, 6551–6557.
31 S. Li, S. Zhang, N. Feng, N. Zhang, Y. Zhu, Y. Liu, W. Wang and X. Xin, *ACS Appl. Mater. Interfaces*, 2022, **14**, 52324–52333.
32 S. Li, N. Feng, M. Sun, Y. Sha, X. Xin, H. Zhao and H. Li, *Nanoscale*, 2024, **16**, 18998–19005.
33 A. Jana, S. Duary, A. Das, A. R. Kini, S. Acharya, J. Machacek, B. Pathak, T. Base and T. Pradeep, *Chem. Sci.*, 2024, **15**, 13741–13752.
34 H. Zheng, Y. Li, W.-W. Zhan, J. Zhou, G. Wu, C. Zhang, D. Sun and Y. Yang, *Angew. Chem., Int. Ed.*, 2025, **64**, e202423787.
35 M. Chang, Y. Xu, Y. Lv, H. Yu, H. Li, X. Kang and M. Zhu, *Chem. Commun.*, 2025, **61**, 11215–11218.

36 T. Jia, P.-M. Cheng, M.-X. Zhang, W.-D. Liu, C.-Y. Li, H.-F. Su, L.-S. Long, L.-S. Zheng and X.-J. Kong, *J. Am. Chem. Soc.*, 2024, **146**, 28618–28623.
37 W.-Q. Shi, L. Zeng, R.-L. He, X.-S. Han, Z.-J. Guan, M. Zhou and Q.-M. Wang, *Science*, 2024, **383**, 326–330.
38 X.-H. Ma, J.-T. Jia, P. Luo, Z.-Y. Wang, S.-Q. Zang and T. C. W. Mak, *Nano Res.*, 2022, **15**, 5569–5574.
39 J. Zhu, R. Zhao, H. Shen, C. Zhu, M. Zhou, X. Kang and M. Zhu, *Aggregate*, 2025, **6**, e720.
40 Y.-J. Kong, Z.-P. Yan, S. Li, H.-F. Su, K. Li, Y.-X. Zheng and S.-Q. Zang, *Angew. Chem., Int. Ed.*, 2020, **59**, 5336–5340.
41 M.-M. Zhang, X.-Y. Dong, Z.-Y. Wang, H.-Y. Li, S.-J. Li, X. Zhao and S.-Q. Zang, *Angew. Chem., Int. Ed.*, 2020, **59**, 10052–10058.
42 Y.-E. Shi, J. Ma, A. Feng, Z. Wang and A. L. Rogach, *Aggregate*, 2021, **2**, e112.
43 Y. G. Srinivasulu, N. Goswami, Q. Yao and J. Xie, *J. Phys. Chem. C*, 2021, **125**, 4066–4076.
44 Y. Jin, Q.-C. Peng, J.-W. Xie, K. Li and S.-Q. Zang, *Angew. Chem., Int. Ed.*, 2023, **62**, e202301000.
45 C. Zhang, W.-D. Si, Z. Wang, A. Dinesh, Z.-Y. Gao, C.-H. Tung and D. Sun, *J. Am. Chem. Soc.*, 2024, **146**, 10767–10775.
46 X. Lin, J. Tang, C. Zhu, L. Wang, Y. Yang, R. A. Wu, H. Fan, C. Liu and J. Huang, *Chem. Sci.*, 2023, **14**, 994–1002.
47 Y. Wang, Z. Zuo, Z. Wang, Y. Wu, J. Linghu, Y. Liu, H. Zhu, X. Dou, T. Feng and X. Yuan, *Chem. Eng. J.*, 2024, **492**, 152216.
48 L. L.-M. Zhang and T. C. W. Mak, *Angew. Chem., Int. Ed.*, 2017, **56**, 16228–16232.
49 T. Chen, S. Yang, J. Chai, Y. Song, J. Fan, B. Rao, H. Sheng, H. Yu and M. Zhu, *Sci. Adv.*, 2017, **3**, e1700956.
50 J.-S. Yang, L.-Y. Xiao, F. Liu, J. Xu, X.-Y. Dong, J.-H. Hu, J. Li and S.-Q. Zang, *Inorg. Chem. Front.*, 2025, **12**, 1420–1426.
51 S. Nematulloev, R.-W. Huang, J. Yin, A. Shkurenko, C. Dong, A. Ghosh, B. Alamer, R. Naphade, M. N. Hedhili, P. Maity, M. Eddaoudi, O. F. Mohammed and O. M. Bakr, *Small*, 2021, **17**, 2006839.
52 D. Liu, G. Gao, Y. Zhang, Q. Li, S. Yang, J. Chai, H. Yu and M. Zhu, *Chem. Commun.*, 2024, **60**, 1337–1340.
53 H. Nie, Y. Han, Z. Tang, S. Yang and B. Teo, *J. Cluster Sci.*, 2018, **29**, 837–846.
54 CCDC 2468154: Experimental Crystal Structure Determination, 2025, DOI: 10.5517/ccdc.csd.cc2nv9wq.